Eur. Phys. J. Plus (2023) 138:704
https://doi.org/10.1140/epjp/s13360-023-04306-5

THE EUROPEAN
PHYSICAL JOURNAL PLUS

Regular Article

Analytical study of low energy proton interactions in the SORGENTINA's fusion ion source-part I: beam-dump

A. Pietropaolo[1,a], **A. Del Dotto**[2], **G. M. Contessa**[3], **the SRF-Collaboration**

[1] Department of Fusion and Technologies for Nuclear Safety and Security, ENEA, Rome, Italy
[2] Frascati National Laboratories, Istituto Nazionale di Fisica Nucleare (INFN), Frascati, Italy
[3] Italian National Institute of Health (ISS), Rome, Italy

Received: 5 May 2023 / Accepted: 20 July 2023

Abstract An analytical study, corroborated by Monte Carlo simulations, is presented which describes the interaction of a 300 keV–830 mA proton beam with a Cu and Al dumping system. The analytical calculations rely on the theoretical framework of the Particle Induced X-ray Emission, while the Monte Carlo simulations are performed by means of the GEANT4 toolkit. The case study is related to the project SORGENTINA-RF fusion neutron source and in particular to the tests devoted to assess the performance of the ion source of the plant. The results provide a detailed physical insight of the main processes occurring in the beam dump material, and are also important to give some realistic figures of the radiation emission expected during operation.

1 Introduction

The ENEA project SORGENTINA-RF will rely on a rotating target where a mixed (50:50) deuteron and triton continuous beam, impinging on a rotating target with a nominal energy of $E_B = 300\,\text{keV}$, spot diameter of about 12 cm and total beam current $I_B \simeq 830\,\text{mA}$. The beam will be directed to a thin (about 3 μm) titanium coating layer covering the rotating target where deuterons and tritons of the beam are implanted, in turn producing fusion neutrons via D–T, D–D and T–T reactions [1].

The first phase of the SORGENTINA-RF project consists in designing and operating the so-called thermo-mechanical demonstrator (TMD). The TMD is composed by a rotating target and an ion source that provides the 250 kW beam power to be extracted by means of a cooling system specially designed for this purpose. Before being coupled to the rotating target, the ion source will be commissioned as a single component, to assess its performance in terms of ion beam spot homogeneity and stability over hundreds of hours in continuous operation. In this phase, the ion source will operate with hydrogen ions with the aim of delivering power without producing neutrons. This test will be thus performed using a proton beam dump designed and constructed on purpose. The material of the dump is still subject to investigation, nevertheless the two main options are copper (Cu) and aluminum (Al) because of their good heat exchange properties and because the final SORGENTINA-RF target will likely be made of one of these two materials. This choice relies on both a preliminary neutronic analysis of possible nuclear heating effects and a minimisation of radioactive waste production [1, 2]. In this context, although new physics phenomena are not involved, nevertheless the PIXE (Particle Induced X-ray Emission) theory is used in a not standard framework and it is instrumental for the development of a 14 MeV neutron source that represents the first of a kind. As already discussed [1], the power density on the rotating target is expected to be lower than 1 MW m^{-2} in operation. As the beam dump is a fixed component, to guarantee the same power density, the proton beam will impinge at a grazing angle onto the dump; the angle was chosen to be 20°.

Against this backdrop, an analytical model was developed with the aim of studying the interaction of low energy protons with the beam dumping system. The analytical approach was validated by Monte Carlo calculations performed with the GEANT4 simulation toolkit. A deeper investigation of the effects of proton interactions with the accelerators' structure is required to avoid undesired personal and environmental exposure as well as processes that may jeopardise the ion source's performance. This topic is typically faced at different proton energy ranges (above several tens of MeV) [3] with respect to the one of interest in this specific case. Little research has been dedicated to the interaction of very low energy protons and the resulting possible radiation protection issues. Generally, this kind of analysis is carried out by means of Monte Carlo simulations, while, in the present study, both analytical and numerical approaches are exploited. The aim is to describe in detail the interaction of the ion beam with the main components of the testing plant, namely the beam dump and the drift tube's residual gas. The benefit of our approach is twofold: first, analytical calculations have the potential to provide a unique insight into the origin of the physical mechanisms involved in the interaction

[a] e-mail: antonino.pietropaolo@enea.it (corresponding author)

Published online: 11 August 2023

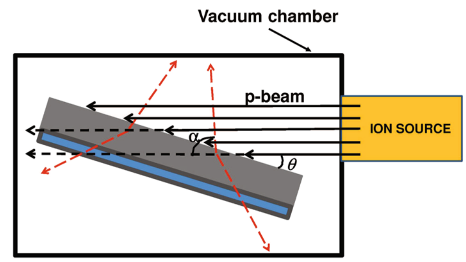

Fig. 1 (Color online) Schematic drawing of the proton beam dump. The incidence angle of the beam is θ=20°. The blue region indicates the water cooling. The red arrows define the X-rays emitted upon proton impact. The angle α is the angle of X-rays emission with respect to the incident proton direction

processes. Second, a detailed comparison between the analytical and numerical results has proved useful to test the reliability of the most recent physics models provided in GEANT4 when treating low energy proton PIXE effects in materials.

The analysis is divided two parts, regarding the two different processes under investigation: Part I deals with the ion beam-dump interactions, Part II with the ion beam-gas interactions. The present manuscripts is related to Part I.

2 Methodological approach to the problem

As far as the analytical approach is concerned, at the energy of the ion source foreseen for the SORGENTINA-RF project [1], one can model the subtending processes with the theoretical framework of PIXE [4].

As regards the simulations, the electromagnetic interaction of the 300 keV protons from the ion source with the beam dump has been carried by means of the GEANT4 code, a single-particle tracker which takes into account all the fundamental interactions of radiation with matter [5–7]. For this specific case study, atomic relaxation processes are simulated by exploiting the most recent updates of GEANT4 releases, which include options for low energy electromagnetic interactions. Atomic de-excitation (fluorescence, Auger electron emission, including Auger cascades and Particle Induced X-ray Emission) can be activated by processes producing vacancies in atomic shells [8]. Processes inducing atomic relaxation in GEANT4 are photoelectric effect, Compton scattering and ionization. The default implemented library describing the atomic relaxation back to neutrality is the Livermore Evaluation Atomic Data Library EADL [9]. Data in EADL include the radiative and non-radiative transition probabilities for each sub-shell of each element, for Z = 1 to 100. The EADL data are used to calculate the complete radiative and non-radiative spectrum of X-rays and electrons emitted, as the atoms relax back to neutrality. When implementing the proton-dump interaction the following aspects of the process have been included in the simulation: (1) geometry of the dumping system, (2) material involved, (3) particle beam of interest (protons), (4) tracking of particles through materials and surrounding spaces, and (5) physical processes subtending the particle interactions, including the de-excitation processes mentioned above.

3 Low energy proton interaction in copper and aluminium in the beam dump

3.1 Ionization processes in the beam dumping system

The electromagnetic interaction of the 300 keV protons from the ion source passing through the beam dump material (see Fig. 1) takes place almost exclusively in terms of ionization, as bremsstrahlung is highly unlikely at this proton energy [10]. Protons interacting with the material transfer their energy E_p (via electromagnetic interaction) to the inner-shell electrons in turn producing ionization. In a first approximation, the number of ionizations $N_{(ion,\,j)}(E_p)$ produced in a given shell j ($j = K,\ L,\ M,\ \ldots$) of a given atomic species in the target can be written as [4]:

$$N_{(ion,j)}(E_p) = \sigma_{(ion,j)}(E_p) \cdot N_Z \cdot t \cdot N_p \tag{1}$$

i.e. proportional to the target concentration (atoms per unit volume), N_Z, of that atomic species, and the number of particles in the beam, N_p, passed through the target of thickness t. The term $\sigma_{(ion,\,j)}(E_p)$ is the ionization cross section for the $j-th$ atomic shell and provides the probability for the interaction to give rise to the specific ionization.

3.2 X-ray emission probability inside the beam dump system

The probability of X-ray emission following an ionization event is measured in terms of the cross section for $j-th$ shell emission, $\sigma_{(X,\,j)}(E_p)$. The ionization and X-ray emission cross sections are related by:

$$\sigma_{(X,j)}(E_p) = \sigma_{(ion,j)}(E_p) \cdot \omega_j \tag{2}$$

ω_j being referred to as the fluorescence yield, *i.e.* the ratio of the number of X-ray emissions to the total number of ionizations produced in the $j-th$ shell [4]. The fluorescence yield for a given atomic shell shows a dependence on the atomic number Z of

Fig. 2 (Color online) Fluorescence yield, ω, as a function of the atomic number, Z, for K- and L-shell emission. *Source*: Ref. [4]

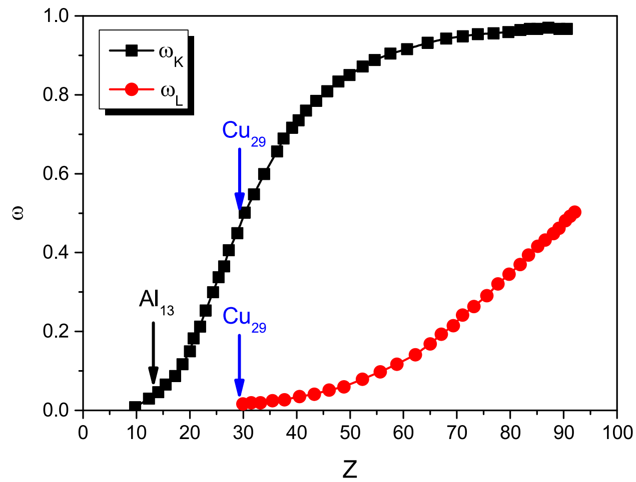

Fig. 3 X-ray emission cross section as a function of the proton energy for Al_{13} in a double log scale: the dashed line is a linear interpolation to determine the cross section value at 300 keV [11]

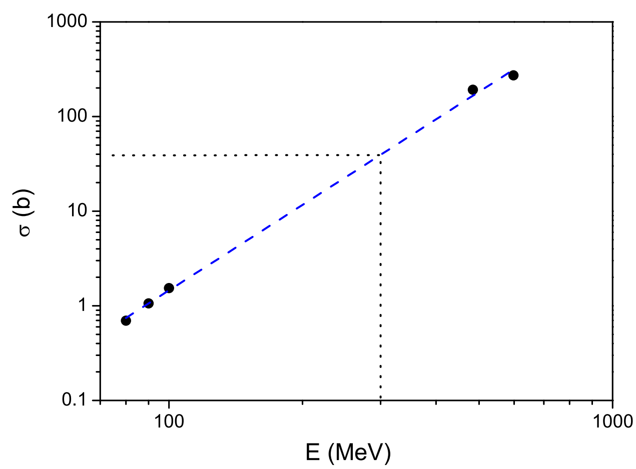

Table 1 Mean values for X-ray emission cross sections of y = Al_{13} and Cu_{29} considering the set of data in Refs. [11, 12]

y	$\overline{\sigma}_{(X,K)}(E_p)$ (b)
Al_{13} [11]	54.2 ± 12.6
Al_{13} [12](*)	61.7 ± 10.7
Al_{13} [12]+ [11]	75.3 ± 2.8
Cu_{29} [11]	0.0783 ± 0.0475
Cu_{29} [12](*)	0.0821 ± 0.0100
Cu_{29} [12]+ [11]	0.0965 ± 0.00361

(*) Average value of $\overline{\sigma}_{(X,K)}(E_p)$
Mean value and uncertainty of $\sigma_{(X,K)}(E_p)$ were calculated using a weighted averaging over the available values

the material being traversed by the proton, as shown in Fig. 2. As it can be noted in Fig. 2, for aluminum (Z = 13) only K-shell emission must be taken into account, and the same is true for copper (Z = 29) because its L-shell emission is practically negligible with respect to the overwhelming K-shell emission.

Values of $\sigma_{(X,K)}(E_p)$ and $\sigma_{(ion,K)}(E_p)$ and ω_K were extracted from Refs [11, 12] for both Cu and Al. When the value of the cross section at $E_p = 300\,\text{keV}$ value was not provided, it was extracted by means of a linear interpolation of data, by plotting $\log[\sigma_{(X,K)}(E_p)]$ vs $\log(E_p)$ as suggested in Ref. [11]. An example of this procedure is shown in Fig. 3. This way, one obtains a set of $\sigma_{(X,K)}(E_p = 300\,\text{keV})$ values from different bibliographic sources, in turn determining the mean values, $\overline{\sigma}_{(X,K)}(E_p)$, and the corresponding uncertainty.

Table 1 provides the final values of $\overline{\sigma}_{(X,K)}(E_p)$ for Al (Z = 13) and Cu (Z = 29) calculated from the databases of Refs. [11, 12]. Also, a cross analysis was done by using the $\sigma_{(ion,j)}(E_p)$ from Ref. [12] and ω_K from Ref. [11] in order to have a wide range of values of $\sigma_{(X,K)}(E_p)$ to be compared.

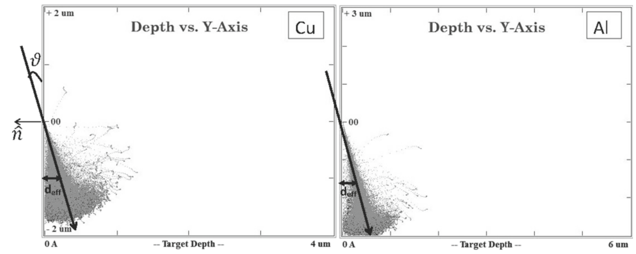

Fig. 4 Result of a TRIM [13] calculation to determine the 300 keV proton range $\Re$ for an incidence angle of $\vartheta = 20°$ with respect to the normal to the dump surface. It shows that, within a simulation cell $4 \times 4\,\mu m^2$ (Cu) and $6 \times 6\,\mu m^2$ (Al), the range is between 2 and 3 μm in both cases, while the lateral straggling is lower than 1 μm (main dark grey zone)

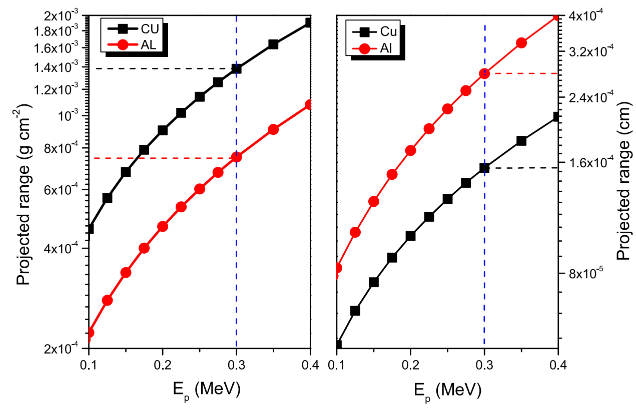

Fig. 5 (Color online) Trend of the proton range $\Re_{(E_p)}$ in units of $cm^2\,g^{-1}$ (left panel) and cm (right panel) for Al_{13} and Cu_{29} as a function of the proton energy. Dashed lines identify the proton energy of interest (300 keV) and the corresponding value of $\Re$ in the plots. Data taken from Ref. [13]

Using the values of $\sigma_{(X,K)}(E_p)$ listed in Table 1 and Eq. (1), the X-ray emission rate can be written as:

$$\frac{d\psi(Z,E_p)}{d\tau} = \overline{\sigma}_{(X,K)}(Z,E_p) \cdot \frac{\rho_y N_A}{A_y} \cdot t \cdot \frac{I_B}{e} \tag{3}$$

I_B being the ion source beam current, e the electron charge ($e = 1.60217662 \times 10^{-19}$ C), N_A the Avogadro's number ($6.023 \times 10^{23}\,mol^{-1}$), while A_y and ρ_y are the atomic mass and the density of the material (the suffix y refers to Al or Cu).

Defining τ_{irr} as the beam-dump irradiation time, the total amount of X-rays emitted by the material interacting with the proton beam is provided by integrating Eq. (3) as follows:

$$\begin{aligned} N_{(X,K)y}(Z,E_p) &= \int_0^{\tau_{irr}} \frac{d\psi(Z,E_p)}{d\tau} d\tau \\ &= \overline{\sigma}_{(X,K)}(Z,E_p) \cdot \frac{\rho_y N_A}{A_y} \cdot t \cdot \frac{I_B}{e} \cdot \tau_{irr} \end{aligned} \tag{4}$$

Therefore, Equation (4) represents the total number of X-rays produced over the irradiation time, in the assumption of a time-independent process. This is valid as the dump is grounded and thus the onset of the braking sheath induced by an excess of positive charges is inhibited.

3.3 X-ray emission rate inside the beam dumping system

In order to proceed further with the calculation, additional considerations have to be done to estimate the "effective thickness", t, that appears in Eq. (3). It is worth to consider that 300 keV protons feature a very small range $\Re_y(E_p)$ into both Cu and Al. A very rough calculation made using the SRIM code [13] provides $\Re_{Al} \simeq 2.8\,\mu m$ and $\Re_{Cu} \simeq 1.5\,\mu m$ for $E_p = 300$ keV (see Fig. 4). Figure 5 shows the variation of the proton range in Al and Cu as a function of the proton energy.

The $\overline{\sigma}_{(X,K)}(E_p)$ can be used to estimate the proton's mean free path, $\lambda_{X-ray}(y_Z)$, for the PIXE process:

$$\lambda_{X-ray}(E_p, y) = \frac{A_y}{N_A \cdot \rho_y \cdot \overline{\sigma}_{(X,K)}(E_p)} \tag{5}$$

From Eq. (5) one obtains, for $E_p = 300$ keV, $\lambda_{X-ray}(E_p) = 0.3$ cm and $\lambda_{X-ray}(E_p) = 160$ cm for Al and Cu, respectively.

Given that $\Re_{(E_p)} \ll \lambda_{X-ray}(E_p)$ for both Al and Cu, the X-ray emission is equiprobable along $\Re(E_p)$ in both cases. In this condition, the mean value of the emission point is $\frac{\Re(E_p)}{2} \pm \frac{\Re(E_p)}{\sqrt{12}}$. Thus, as it can be noted from Fig. 4, the effective layer $d_{eff}(E_p)$ from which the X-ray emission takes place is smaller than 1 μm, i.e. $d_{eff}(E_p) = \frac{\Re_y(E_p)}{2} \cdot sin(\vartheta)$ (y = Al or Cu), that provides 0.23

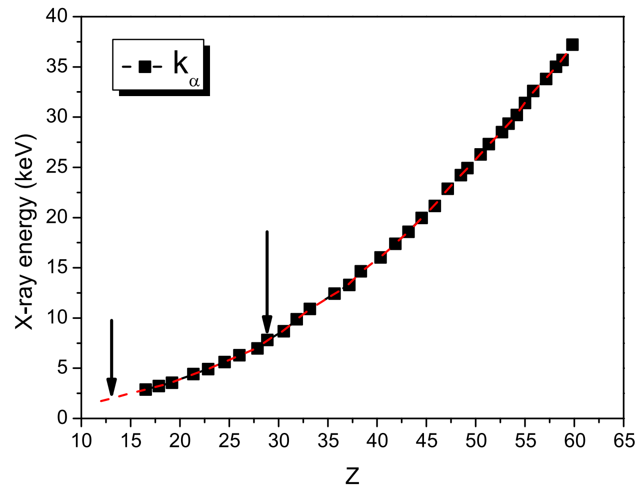

Fig. 6 (Color online) Energies of the Kα X-rays as a function of the atomic number (Z) of the element [4].The arrow indicate $Z = 13$ and 29, i.e.Al and Cu respectively

μm for Al and about $= 0.13\,\mu$m for Cu. For the above mentioned considerations, Eq. (3) can be rewritten replacing t with $d_{eff}(E_p)$, in turn obtaining:

$$\frac{d\psi(Z,E_p)}{d\tau} = \overline{\sigma}_{(X,K)}(Z,E_p)\cdot\frac{\rho_y N_A}{A_y}\cdot\frac{\Re_y(E_p)}{2}\cdot sin(\vartheta)\cdot\frac{I_B}{e} \tag{6}$$

By substituting for $\overline{\sigma}_{(X,K)}(Z, E_p)$ the largest value in Table 1 for Al ad Cu (conservative hypothesis) and the correct values of the other quantities into Eq. (6), one finds:

$$\left(\frac{d\psi}{d\tau}\right)_{Al} = 7\times 10^{14} s^{-1} \tag{7}$$

and

$$\left(\frac{d\psi}{d\tau}\right)_{Cu} = 6.2\times 10^{11} s^{-1} \tag{8}$$

These figures represent an upper limit, as no self-shielding effect was taken into account in the calculation.

3.4 X-ray emission rates from the beam dumping system

With the aim of determining the X-ray emission rate from the beam dump system to the closed outside region, Eq. (3) has to be rewritten taking into account the transmission probability through the beam dump layer. To this aim, one should consider that the typical PIXE energy for Al and Cu is approximately 2 keV and 7 keV respectively, as it can be seen from Fig. 6 showing the dependence of the photon energy as a function of the atomic number Z [4, 14].

A very rough calculation can be made using the XCOM database [15] to determine the attenuation mean free path, $\lambda_{att}(E_{ph})$, for $E_{ph} = 2$ and 7 keV photons in Al and Cu, respectively. XCOM provides the attenuation coefficient $\mu(E_{ph})$ in materials as a function of the photon energy, as shown in Fig. 7.

Thus, once the density of the material ρ (g cm^{-3}) is known, the photon mean free path in the material is $\lambda_{att}(E_{ph}) = [\mu(E_{ph})\cdot\rho]^{-1}$. By means of $\lambda_{att}(E_{ph})$ one can estimate the transmission probability for the specific material $\mathcal{T}(E_{ph}, E_p)$ as:

$$\mathcal{T}(E_{ph},E_p) = exp\left(-\frac{d_{eff}(E_p)}{\lambda_{att}(E_{ph})}\right) \tag{9}$$

E_{ph} being the photon energy. Considering Eqs. (9) and (3), the X-ray emission rate from the beam dump layer is given by:

$$\left[\frac{d\psi(Z,E_p)}{d\tau}\right]_{att} = \mathcal{T}(E_{ph},E_p)\cdot\frac{d\psi(Z,E_p)}{d\tau} \tag{10}$$

Indeed, this represents an upper limit, as the attenuation effect on the X-ray emission is considered isotropic, $i.e.$ neglecting the different degree of X-ray self-shielding as these traverse the beam dump along sections of different thickness (see Fig. 1). Thus, the overestimation comes from neglecting geometrical effects defined by a directional attenuation probability $\mathcal{T}(E_{ph}, E_p, \alpha)$, with α being the emission angle with respect to a defined direction, such as the incident proton direction. Considering the values of d_{eff} and λ_{att}, one obtains $[\mathcal{T}(E_{ph}, E_p)]_{Al} = 0.75$ and $[\mathcal{T}(E_{ph}, E_p)]_{Cu} = 0.98$. In this framework, one obtains the X-ray emission rate from the beam dumping system:

$$\left[\frac{d\psi(Z,E_p)}{d\tau}\right]_{att} \simeq (5.2\pm 1.7)\times 10^{14} s^{-1} \tag{11}$$

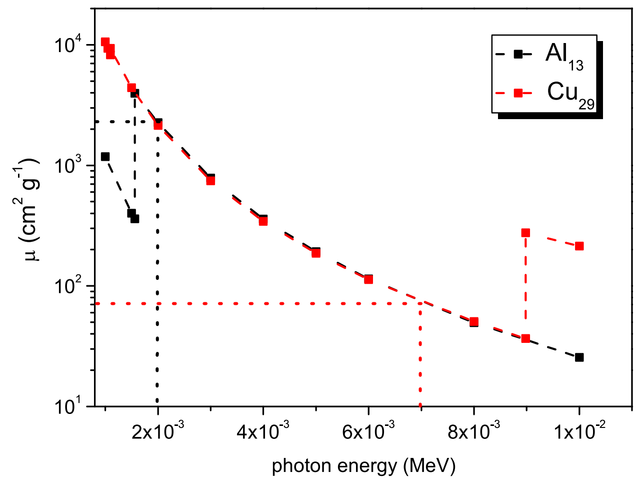

Fig. 7 Attenuation length in units of cm^2 g^{-1} for Al_{13} and Cu_{29} as a function of the photon energy. The dashed lines refer to the Kα X-rays from Al_{13} (2 keV) and Cu_{29} (7 keV). See Fig. 6

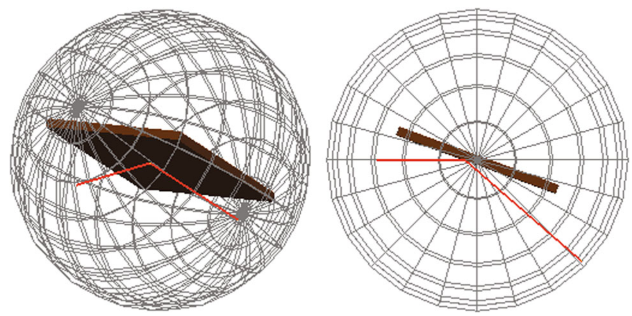

Fig. 8 (Color online) Geometry used for the GEANT4 simulations: the dump (in dark brown), a spherical shielding chamber made of steel (in grey) and the proton beam (in red) at 20° with respect to the dump surface normal direction

for aluminum and

$$\left[\frac{d\psi(Z, E_p)}{d\tau}\right]_{att} \simeq (6.1 \pm 2.0) \times 10^{11} s^{-1} \tag{12}$$

for copper.

The uncertainty in Eqs. (11) and (12) is given by the sum of the uncertainty on the cross section used in the calculation (about 4%) and the one on the proton range (about 29%), providing an overall uncertainty of about 33%.

3.5 X-rays attenuation in the vacuum chamber

The last step is the estimation of the attenuation power of the vacuum chamber where the beam dump will be inserted for the testing activity (see Fig. 1). The flux of X-rays emerging from the vacuum chamber is the relevant quantity in relation to the protection of workers and the members of the public. From the technical specifications of the project, the material of the vacuum chamber is chosen to be steel (density $\rho_s = 8.05$ g cm^{-3}) with a thickness of 3 mm. In order to provide an approximated value of the attenuation coefficient μ using the XCOM database [15], one can assume that the major contribution to μ comes from Fe, which represents about 98.7% in the steel composition. The value of μ_{Fe} is 1.623×10^3 cm^2 g^{-1} for the Al X-rays at 2 keV, while it is 3.04×10^2 cm^2 g^{-1} for the 7 keV X-rays from Cu. In terms of mean free path $\lambda = (\mu \cdot \rho)^{-1}$ one obtains $\lambda_{Fe}(2\text{ keV}) \simeq 7.8 \times 10^{-5}$ cm and $\lambda_{Fe}(7\text{ keV}) \simeq 4.2 \times 10^{-4}$ cm. These values of the mean free path provide the transmission coefficients for steel $\mathcal{T}(E_{ph} = 2\text{ keV}) = \mathcal{T}(E_{ph} = 7\text{ keV}) \simeq 0$. This means that outside the beam dump, for both 2 and 7 keV X-rays, the X-ray count rate is practically

$$\left(\frac{d\psi}{d\tau}\right)_{out} \simeq 0. \tag{13}$$

4 Monte Carlo simulations

Figure 8 shows the resulting tracks of the primary proton beam hitting the dump, which is supposed to be 5 mm thick and surrounded by a steel chamber of 3 mm thickness.

Simulations have been performed both with copper and aluminum dumping material. Figure 9 shows the spectra of the X-rays emitted per unit time from the beam dump layer, $[\frac{dN(Z,E_p)}{d\tau}]_{att}$ (see Eqs. 11 and 12).

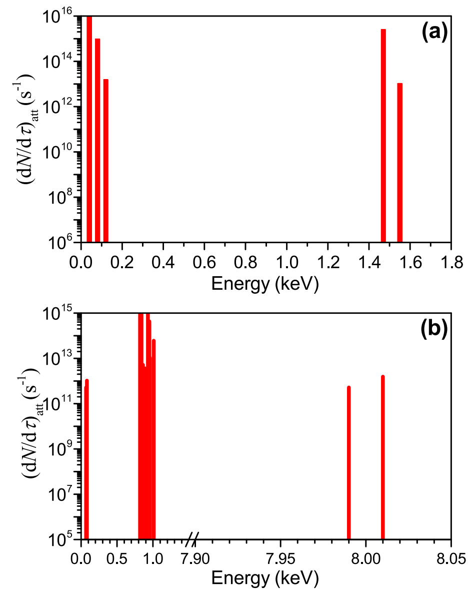

Fig. 9 (Color online) Spectra of the X-rays produced within the aluminum (**a**) and the copper (**b**) beam dump

For the X-ray emission lines closest to those considered for the analytical calculations (2 keV and 7 keV for Al and Cu, respectively), the numerical calculations provide,:

$$\left[\frac{d\psi(Z, E_p)}{d\tau}\right]_{att,Al} = (2.5 \pm 0.1) \times 10^{15} s^{-1} \tag{14}$$

for aluminum and

$$\left[\frac{d\psi(Z, E_p)}{d\tau}\right]_{att,Cu} = (2.1 \pm 1.5) \times 10^{12} s^{-1} \tag{15}$$

for copper. The total number of simulated histories is 10^7 for both Al and Cu cases. This provides an uncertainty estimate of 4% for the Al case (Eq. 14) and 70% for Cu case (Eq. 15). This difference reflects the huge one between Al and Cu PIXE cross sections (see Table 1).

As far as the shielding effect of the vacuum chamber is concerned, the Monte Carlo calculation provides no particles outside the chamber, within the statistical sensitivity of the simulation over 10^7 proton histories considered.

5 Comparison and discussion

With the objective of estimating the X-ray emission rate from the dump layer, in the analytical approach the characteristic X-ray energies of 2 keV (Al) and 7 keV (Cu) were used providing the values in Eqs. (11) and (12). Inspection of Fig. 9 shows that the X-ray energies used in the analytical calculations well approximate those calculated by the Monte Carlo.

Regarding the X-ray emission rate from the dump layer, both analytical and Monte Carlo calculations (Eqs. 11–15) provide a lower rate for Cu of about three orders of magnitude that reflects the lower X-ray emission cross section (see Table 1).

Interestingly, using the uncertainty figures, MC simulations (Eqs. 14 and 15) and analytical calculations (Eqs. 11 and 12) differ by a factor of 3 for Al while are consistent for Cu within 1σ.

The differences between the two approaches is most likely due to unavoidable sources of uncertainties. The major sources of uncertainties are identified and discussed below:

- In the analytical calculation, the values for X-ray emission cross sections were extrapolated from data in literature (e.g. Fig. 3) with appreciable uncertainties (Table 1); the Monte Carlo calculates emission probabilities over randomly selected proton energies picking cross section values from its data library.
- In the analytical approach, a single X-ray emission point was assumed within the dump layer (d_{eff} in Fig. 4); Monte Carlo provides for each proton the contributions to the X-rays emission from randomly chosen points visited by the proton along its track in the dump.
- In the analytical calculation the choice of the single emission point at d_{eff} also affects the estimate of the emission probability (Eq. 6), as the cross section varies with the energy of the incident proton, which, in turn, depends on the length travelled in the medium.

Then, the slightly higher X-ray emission rates in the Monte Carlo calculations are reasonably explained on the basis of the previous considerations on the sources of discrepancy.

6 Conclusions

The ENEA project SORGENTINA-RF will start with a pilot phase for testing and validating the design of the ion source. To this aim, the ion source will operate in hydrogen with the beam directed toward a Cu or Al beam dump without producing neutrons. An analytical calculation is here presented to investigate the interaction of the 300 keV proton beam with the material of the beam dump and to determine the expected X-ray emission. This calculation is done relying on the theoretical framework of Particle Induced X-ray Emission. The continuous slowing-down approximation is supposed: the protons are assumed to lose their energy continuously along their tracks and the major energy-loss mechanisms considered to be significant are inelastic collisions with the electrons in the absorbing medium, thus resulting primarily in the ionization and excitation of atoms. As the project is in the design phase, in the calculation both copper and aluminum are considered as constituent materials of the beam dump.

In relation to the mechanisms under study, the number of ionizations and the mean value of the X-ray emission point are evaluated on the basis of statistical considerations, and the X-rays emission results to be completely shielded by the vacuum chamber foreseen to be used for the experiment.

Analytical calculations and Monte Carlo simulations are found in satisfactory agreement considering the assumptions hypothesized in the analytical model.

Given that SORGENTINA-RF will be the first of a kind, Monte Carlo simulations are a valuable tool to obtain accurate figures. Likewise, the analytical approach highlights and provides physical insight into the main phenomena involved and test the results obtained with the most recent GEANT4 release used in the present study. The outcomes are also relevant in relation to the protection and safety of the operators of the facility when testing the ion source.

Further studies will be developed to estimate the potential radiation emission from other components of the ion source during its operations, with the aim of the safety and radiation protection of the operators and of the design of the ancillary structures of the facility.

Acknowledgements The authors warmly acknowledge Dr. G. Celentano (ENEA), Dr. A. Doria (ENEA) and Dr. F. Consoli (ENEA) for precious discussions and indications. The authors acknowledge the Regione Emilia Romagna-ENEA agreement for the project "SORGENTINA RF - Thermomechanical Demonstration".

The SRF Collaboration: Pietro Agostini (ENEA - Department of Fusion and Technologies for Nuclear Safety and Security, Italy, pietro.agostini@enea.it), Massimo Angiolini (ENEA - Department of Fusion and Technologies for Nuclear Safety and Security, Italy, massimo.angiolini@enea.it), Ciro Alberghi (Politecnico di Torino, Italy, ciro.alberghi@polito.it), Luigi Candido (Politecnico di Torino, Italy, luigi.candido@polito.it), Marco Capogni (ENEA - Department of Fusion and Technologies for Nuclear Safety and Security, Italy and ENEA - Italian National Institute of Ionizing Radiation Metrology, Italy, marco.capogni@enea.it), Mauro Capone (ENEA - Department of Fusion and Technologies for Nuclear Safety and Security, Italy and ENEA - Italian National Institute of Ionizing Radiation Metrology, Italy, mauro.capone@enea.it), Sebastiano Cataldo (ENEA - Department of Fusion and Technologies for Nuclear Safety and Security, Italy, sebastiano.cataldo@enea.it), Gian Marco Contessa (Italian National Institute of Health (ISS) - Roma, Italy, gianmarco.contessa@iss.it), Marco D'Arienzo (ASL Roma 6, Borgo Garibaldi, 12, 00041 Albano Laziale (RM), marco.darienzo77@gmail.com), Danilo Nicola Dongiovanni (ENEA - Department of Fusion and Technologies for Nuclear Safety and Security, Italy, danilo.dongiovanni@enea.it), Paolo Ferrari (ENEA - Radiation Protection Institute, Italy, paolo.ferrari@enea.it), Davide Flammini (ENEA - Department of Fusion and Technologies for Nuclear Safety and Security, Italy, davide.flammini@enea.it), Nicola Fonnesu (ENEA - Department of Fusion and Technologies for Nuclear Safety and Security, Italy, nicola.fonnesu@enea.it), Manuela Frisoni (ENEA - Department of Fusion and Technologies for Nuclear Safety and Security, Italy, manuela.frisoni@enea.it), Gianni Gadani (ENEA - Department of Fusion and Technologies for Nuclear Safety and Security, Italy, gianni.gadani@enea.it), David Guidoni (ENEA - Management of infrastructures and services, Italy, david.guidoni@enea.it), Marco Lamberti (ENEA - Department of Fusion and Technologies for Nuclear Safety and Security, Italy, marco.lamberti@enea.it), Luigi Lepore (ENEA - Department of Fusion and Technologies for Nuclear Safety and Security, Italy, luigi.lepore@enea.it), Andrea Mancini (ENEA - Department of Fusion and Technologies for Nuclear Safety and Security, Italy, andrea.mancini@enea.it), Ranieri Marinari (ENEA - Department of Fusion and Technologies for Nuclear Safety and Security, Italy, ranieri.marinari@enea.it), Giuseppe A. Marzo (ENEA - Department of Fusion and Technologies for Nuclear Safety and Security, Italy, giuseppe.marzo@enea.it), Bruno Mastroianni (ENEA - Management of infrastructures and services, Italy, bruno.mastroianni@enea.it), Fabio Moro (ENEA - Department of Fusion and Technologies for Nuclear Safety and Security, Italy, fabio.moro@enea.it), Vincenzo Narcisi (ENEA - Department of Fusion and Technologies for Nuclear Safety and Security, Italy, vincenzo.narcisi@enea.it), Agostina Orefice (ENEA - Department of Fusion and Technologies for Nuclear Safety and Security, Italy, agostina.orefice@enea.it), Antonino Pietropaolo (ENEA - Department of Fusion and Technologies for Nuclear Safety and Security, Italy, antonino.pietropaolo@enea.it), Antonietta Rizzo (ENEA - Department of Fusion and Technologies for Nuclear Safety and Security, Italy, antonietta.rizzo@enea.it), Alexander Rydzy (ENEA - Department of Fusion and Technologies for Nuclear Safety and Security, Italy, alexander.rydzy@enea.it), Stefano Salvi (ENEA - Department of Fusion and Technologies for Nuclear Safety and Security, Italy, stefano.salvi@enea.it), Demis Santoli (ENEA - Department of Fusion and Technologies for Nuclear Safety and Security, Italy, demis.santoli@enea.it), Alessia Santucci (ENEA - Department of Fusion and Technologies for Nuclear Safety and Security, Italy, alessia.santucci@enea.it), Luca Saraceno (ENEA - Department Energy Technologies and Renewable Sources, Italy, luca.saraceno@enea.it), Camillo Sartorio (ENEA - Department of Fusion and Technologies for Nuclear Safety and Security, Italy, camillo.sartorio@enea.it), Salvatore Scaglione (ENEA - Department Energy Technologies and Renewable Sources, Italy, salvatore.scaglione@enea.it), Valerio Sermenghi (ENEA - Department of Fusion and Technologies for Nuclear Safety and Security, Italy, valerio.sermenghi@enea.it), Emanuele Serra (ENEA - Department for Sustainability, Italy, emanuele.serra@enea.it), Andrea Simonetti (ENEA - Department of Fusion and Technologies for Nuclear Safety and Security, Italy, andrea.simonetti@enea.it), Ivan Panov Spassovsky (ENEA - Department of Fusion and Technologies for Nuclear Safety and Security, Italy, ivan.spassovsky@enea.it), Nicholas Terranova (ENEA - Department of Fusion and Technologies for Nuclear Safety and Security, Italy, nicholas.terranova@enea.it), Silvano Tosti (ENEA - Department of Fusion and Technologies for Nuclear Safety and Security, Italy, silvano.tosti@enea.it), Alberto Ubaldini (ENEA - Department of Fusion and Technologies for Nuclear Safety and Security, Italy, alberto.ubaldini@enea.it), Konstantina Voukelatou (ENEA - Department of Fusion and Technologies for Nuclear Safety and Security, Italy, konstantina.voukelatou@enea.it), Pietro Zito (ENEA - Department of Fusion and Technologies for Nuclear Safety and Security, Italy, pietro.zito@enea.it), Giuseppe Zummo (ENEA - Department Energy Technologies and Renewable Sources, Italy, giuseppe.zummo@enea.it)

Funding Open access funding provided by Ente per le Nuove Tecnologie, l'Energia e l'Ambiente within the CRUI-CARE Agreement.

Data Availability Statement This manuscript has associated data in a data repository. [Authors' comment: The data sets generated during and/or analysed during the current study are available from the corresponding author on reasonable request.]

References

1. A. Pietropaolo et al., Eur. Phys. J. Plus **136**(11), 1140 (2021)
2. G.M. Contessa et al., Environments **9**, 71 (2022)
3. L.E. Moritz, Rad. Prot. Dosim. **96**, 297 (2001)
4. P. Mandó, W. Przybylowicz, *Encyclopedia of Analytical Chemistry* (Wiley, New York, 2016)
5. S. Agostinelli et al., Nucl. Instr. Meth. A **506**(3), 250 (2003)
6. J. Allison et al., IEEE Trans. Nucl. Sci. **53**(1), 270 (2006)
7. J. Allison et al., Nucl. Instrum. Methods A **835**, 186 (2016)
8. S. Bakr et al., Nucl. Instrum. Methods B **436**, 285 (2018)
9. S.T. Perkins, others, in *Tables and Graphs of Atomic Subshell and Relaxation Data Derived from the Llnl Evaluated Atomic Data Library (eadl), z=1-100*, Technical Report UCRL-50400 Vol.30 (Lawrence Livermore National Lab., CA) (1991)
10. J.D. Jackson, Classical Electrodynamics
11. G. Lapicky, J. Phys. Chem. Ref. Data **18**, 111 (1989)
12. H. Paul, J. Sacher, At. Data Nucl. Data Tables **42**, 105 (1989)
13. http://www.srim.org/
14. W. Bambynek et al., Rev. Mod. Phys. **44**, 716 (1972)
15. https://physics.nist.gov/PhysRefData/Xcom/html/xcom1.html